

TIMED Solar EUV Experiment : pre-flight calibration results for the XUV Photometer System

Thomas N. Woods^a, Erica Rodgers^a, Scott M. Bailey^b, Francis G. Eparvier^a, and Greg Ucker^a

^aLaboratory for Atmospheric and Space Physics, University of Colorado, Boulder, CO 80309-0590

^bHampton University, 23 Tyler St., Hampton, VA 23668

ABSTRACT

The Solar EUV Experiment (SEE) on the NASA Thermosphere, Ionosphere, and Mesosphere Energetics and Dynamics (TIMED) mission will measure the solar vacuum ultraviolet (VUV) spectral irradiance from 0.1 to 200 nm. To cover this wide spectral range two different types of instruments are used: a grating spectrograph for spectra between 25 and 200 nm with a spectral resolution of 0.4 nm and a set of silicon soft x-ray (XUV) photodiodes with thin film filters as broadband photometers between 0.1 and 35 nm with individual bandpasses of about 5 nm. The grating spectrograph is called the EUV Grating Spectrograph (EGS), and it consists of a normal-incidence, concave diffraction grating used in a Rowland spectrograph configuration with a 64 x 1024 array CODACON detector. The primary calibrations for the EGS are done using the National Institute for Standards and Technology (NIST) Synchrotron Ultraviolet Radiation Facility (SURF-III) in Gaithersburg, Maryland. In addition, detector sensitivity and image quality, the grating scattered light, the grating higher order contributions, and the sun sensor field of view are characterized in the LASP calibration laboratory. The XUV photodiodes are called the XUV Photometer System (XPS), and the XPS includes 12 photodiodes with thin film filters deposited directly on the silicon photodiodes' top surface. The sensitivities of the XUV photodiodes are calibrated at both the NIST SURF-III and the Physikalisch-Technische Bundesanstalt (PTB) electron storage ring called BESSY. The other XPS calibrations, namely the electronics linearity and field of view maps, are performed in the LASP calibration laboratory. The XPS and solar sensor pre-flight calibration results are primarily discussed as the EGS calibrations at SURF-III have not yet been performed.

Keywords: ultraviolet instrumentation, satellite instrumentation, solar irradiance instrumentation

1. INVESTIGATION OVERVIEW

The Solar EUV Experiment (SEE) investigation contributes primarily to the NASA TIMED mission goal to characterize the sources of energy responsible for the thermal structure of the mesosphere, the lower thermosphere, and the ionosphere (MLTI). These energy sources include solar radiation, solar energetic particles, Joule heating, conduction, dynamical forcing, and chemical energy release. Of these energy inputs, the solar vacuum ultraviolet (VUV) radiation below 200 nm is the dominant global energy source for heating of the thermosphere, creating the ionosphere, and driving the diurnal cycles of wind and chemistry. Figure 1 shows a complete solar VUV irradiance spectrum that combines the measurements made from our rocket experiment and Upper Atmosphere Research Satellite (UARS) SOLar STellar Irradiance Comparison Experiment (SOLSTICE). This spectrum illustrates the quality and spectral resolution that the TIMED SEE instruments will produce. While solar cycle variability near 200 nm is only about 10%, the solar cycle variability at shorter wavelengths is typically a factor of 2 to 3 for chromospheric emissions and a factor of 10 to 100 for coronal emissions. The variability of both of these emissions are not well understood, especially at the shortest wavelengths below 40 nm. More detailed reviews about the solar extreme ultraviolet (EUV) and ultraviolet (UV) variability include those by Lean^{1,2} and Rottman³. A detailed quantitative understanding of the changes in the solar VUV irradiance and the basic state variables, temperature and densities of N₂, O₂, and O, are essential to detailed investigations of atmospheric energetics, dynamics, and chemistry. The SEE will provide the necessary solar VUV irradiance measurements from 0.1 to 200 nm with about 0.5 nm spectral resolution and with about hourly temporal resolution. These measurement capabilities have been established considering the atmosphere's response to the solar radiation and also considering the characteristics of the solar spectrum and its variability. Other TIMED instruments will provide the measurements of the basic state variables over a range of altitudes from 50 to 300 km. The occasional solar

occultations by SEE also provide precise measurements of the basic state variables. With the accurate measurements of the energy sources and the basic state variables, atmospheric models of the MLTI can be validated and refined in an unprecedented manner, and the response of the upper atmosphere to the various energy sources can be precisely quantified.

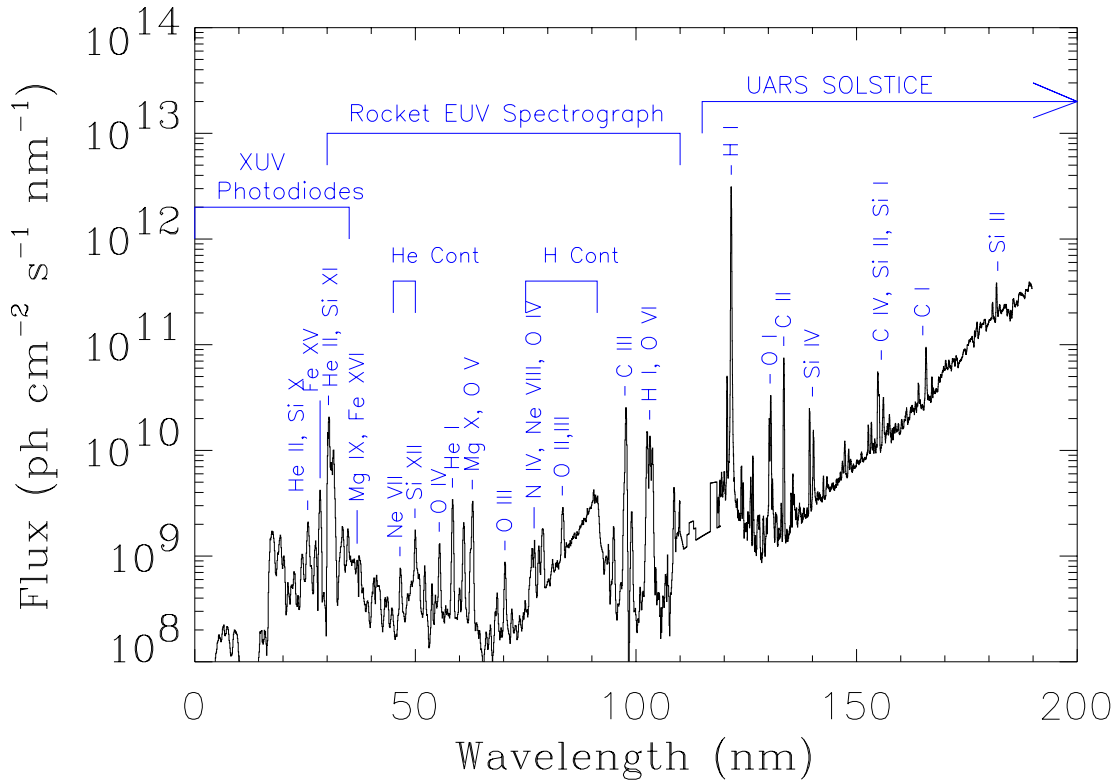


Figure 1. Solar VUV Irradiance Measurement on October 27, 1992. The rocket solar EUV irradiance instruments made the measurements below 110 nm, and the UARS SOLSTICE made the measurements above 119 nm. The SEE solar VUV irradiance measurements will be very similar and will span the entire range from 0.1 to 200 nm.

The SEE investigation also contributes to the TIMED mission goal to improve our understanding of those processes related to anthropogenic influence and to establish a baseline set of observations for future investigations. In order to distinguish between the natural, namely solar variability, and anthropogenic changes in the MLTI regions, a baseline of solar VUV spectral irradiance and basic state variables needs to be established with an accuracy of 10% or better (1- σ value). Existing proxy models that employ ground-based measurement of solar activity to estimate the solar VUV irradiance are highly uncertain and lack the required accuracy for solar connection studies. Therefore, the SEE investigation will also develop improved solar proxy models, based on the TIMED SEE measurements, for future comparisons of natural and anthropogenic effects.

The key elements in data analysis and modeling for the SEE investigation are the analysis of the solar irradiance variability, studying the solar-terrestrial relationships by using the measured solar irradiance as parameters in models of the atmosphere, verification of atmospheric models and laboratory cross sections for atoms and molecules by using measured solar absorption profiles from solar occultations, and development of a new generation proxy model of the solar EUV irradiance. The primary atmospheric models are the Thermosphere-Ionosphere-Mesosphere-Electrodynamics General Circulation Model (TIME-GCM)⁴ and the MSIS model⁵.

2. INSTRUMENTATION

The Solar EUV Experiment (SEE) includes two instruments to measure the solar VUV spectral irradiance from 0.1 to 200 nm. The EUV Grating Spectrograph (EGS) is a normal incidence Rowland circle spectrograph and has a spectral range of 25 to 195 nm with a 0.4 nm spectral resolution. The EGS photon-counting detector is a CODACON array detector (64 x 1024 anodes) which uses microchannel plates (MCP) and coded anode electronics for its readout. The XUV Photometer System (XPS) includes nine silicon XUV photodiodes with thin film filters deposited directly on the photodiode. This XUV photometer set measures the solar irradiance from 0.1 to 35 nm with each filter having a spectral bandpass of about 5 nm. Additional subsystems to accommodate this solar investigation on the TIMED spacecraft include the SEE Solar Pointing Platform (SSPP), a one-axis gimbal platform for pointing the solar sensors towards the Sun, and the Microprocessor Unit (MU). With the SSPP controlling the solar pointing in only 1 axis, the SEE instruments have a wide field of view ($>11^\circ$) so that the Sun can drift through their field of view for a few minutes each orbit. Figure 2 shows the assembled SEE instrument but without its thermal blankets installed. For this paper, we focus the discussion on the pre-flight calibrations for the solar irradiance sensors. A more detailed description of the SEE instrument is given by Woods *et al.*⁶. The SEE instrument was recently delivered for integration on the NASA TIMED spacecraft at the Johns Hopkins University (JHU) Applied Physics Laboratory (APL).

The following characteristics are for the entire SEE system. The mass of SEE is 29 kilograms. The SEE operating power is 30 Watts, and the SEE maximum operating data rate is 4 kilobits per second. Because the normal SEE observation scenario is to observe the Sun autonomously every orbit for only two to four minutes, the SEE orbit average power is lower at about 14 Watts, and the orbit average data rate is about 0.2 kilobits per second. The expected operating temperature range for SEE is 10 to 34 °C. Because SEE has its own pointing platform and Sun sensor, it imposes minimal requirements on the spacecraft attitude control.

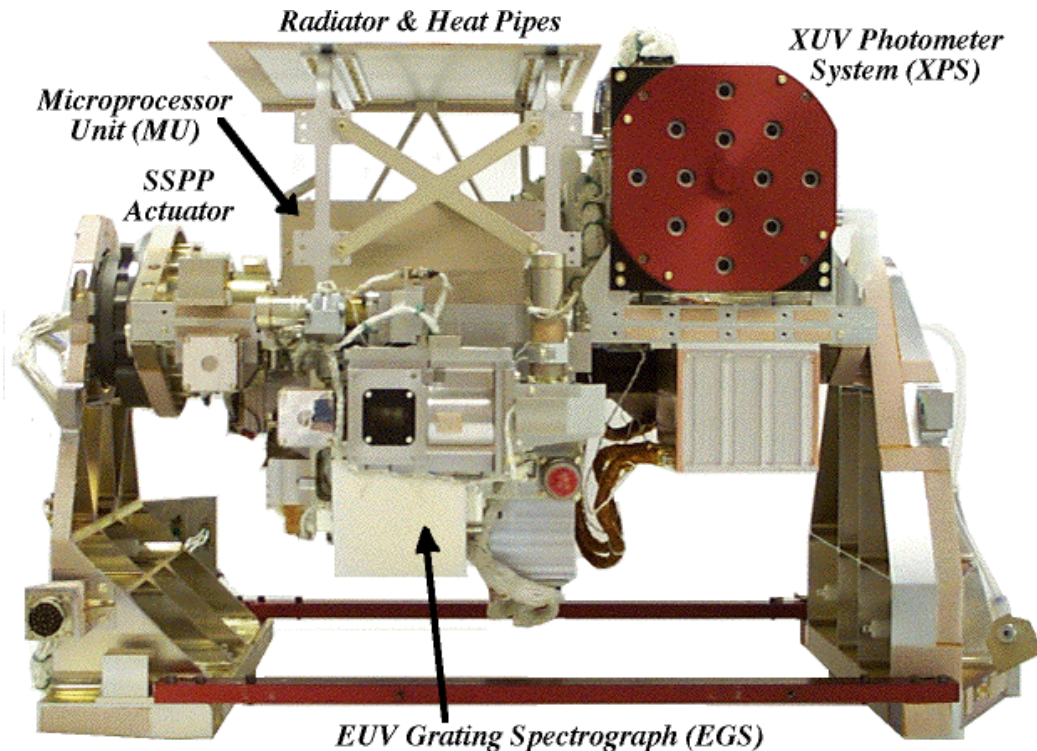


Figure 2. TIMED Solar EUV Experiment Assembled View.

3. CALIBRATION OVERVIEW

One of the critical problems with many of the earlier solar VUV irradiance measurements has been the absolute accuracy of the irradiance and the long-term accuracy related to tracking the instrument degradation. The pre-flight and in-flight calibrations are therefore especially important for the SEE program.

3.1. Pre-flight Calibrations

The pre-flight photometric calibrations of SEE include transferring the calibrations of the National Institute of Standards and Technology (NIST) radiometric standards, such as reference photodiodes, radioactive x-ray sources, and synchrotron radiation, to the instrument^{7,8,9}. The current VUV calibration techniques achieve an accuracy of about 3 to 7% ($1-\sigma$ value).

The individual optical elements, that is the gratings and detectors, are calibrated at the unit level in order to select the best elements for flight. In addition, the fully assembled instrument is calibrated and mapped over its field of view (FOV) to precisely determine the uniformity across its FOV. A careful analysis of the spectrograph's scattered light, which is primarily caused by the diffraction grating, is also performed using laboratory measurements. A blazed, mechanically-ruled grating from Hyperfine is used because holographically-ruled gratings appear inadequate to cover such a wide spectral range.

The primary photometric standard for the SEE calibrations is the Synchrotron Ultraviolet Radiation Facility (SURF-III) at NIST in Gaithersburg, Maryland. The EGS is directly calibrated at SURF, and the XPS photodiodes are calibrated as a function of wavelength at SURF and at the Physikalisch-Technische Bundesanstalt (PTB) electron storage ring called BESSY.

Other pre-flight calibration tests include wavelength calibrations, linearity tests of the detectors and their electronics, scattered light measurements, and detailed mapping of the field of views. The wavelength calibrations for EGS incorporate measurements using emission line sources from deuterium and hollow cathode lamps. The linearity tests for EGS are easily performed using the capability to adjust the SURF electron beam current level over six orders of magnitude. The linearity tests for XPS electronics uses a calibrated, adjustable current source in place of the photodiode. The scattered light measurements are primarily for the SEE grating spectrograph in order to characterize the scattered light properties of the grating. These scattered light tests include unit level tests and system level tests as performed with UARS SOLSTICE^{10,11}. The gimbal tables at SURF is utilized to make detailed FOV maps for EGS as done for the UARS SOLSTICE and solar rocket instruments^{10,12,13}. A $12^\circ \times 12^\circ$ gimbal table at LASP is used to obtain the visible FOV maps for XPS.

3.2. In-Flight Calibrations

In addition to measuring the absolute value of the solar irradiance, determining the long term variation of the irradiance is a fundamental scientific goal; therefore, in-flight calibrations of SEE are required to monitor changes in the instrument response. The in-flight calibration techniques for SEE are on-board photometric standards, redundant measurements by overlapping wavelength regions, redundant optical channels, and underflight calibrations. This variety of in-flight calibration techniques will assure that the SEE long-term accuracy of the solar flux is maintained at or below the desired 10% uncertainty ($1-\sigma$ value).

The XPS serves as an on-board photometric standard as its photodiodes are known to be very stable and have been adopted by NIST as a secondary detector standard^{14,15,16,17,18}. The EGS also benefits from the XPS photometric standard as the EGS and XPS overlap in the 25 to 35 nm region.

Each instrument has redundant optical channels. One channel will be utilized for daily measurements, and one channel will only be used once a week to regularly provide a relative calibration for the other channel. The basic assumption for this technique is that exposure to the space environment and to solar radiation is a major factor determining instrument degradation. By using different duty cycles we can evaluate accurately the degradation related to solar exposure rate. By maintaining a high level of cleanliness for the instruments, as done for UARS SOLSTICE, we expect to greatly reduce the degradation related to contaminants on the optical elements.

Suborbital calibration experiments are of great importance in providing an absolute in-flight calibration on an annual basis. These experiments will be conducted as sounding rocket experiments using the SEE protoflight instrument so that the

spectral resolution of the calibration instruments will be exactly the same as the flight instrument. Pre- and post-flight calibration of the protoflight instrument will be performed at SURF for every calibration rocket flight. These SEE underflight experiments will provide an absolute calibration for both SEE channels. From our experience with UARS SOLSTICE and the rocket instruments, we only expect a degradation rate for the EGS instrument to be a few percent per year. Based on NIST tests and the Student Nitric Oxide Explorer (SNOE) XUV photodiodes¹⁹, we expect a degradation rate for the XPS instrument to be less than a percent per year. These relatively low degradation rates are related to keeping the optics and components free from contaminants (for example, never in an oil-based vacuum system) and to using very small apertures in order to limit the exposure to solar radiation. With the expected low degradation rate and because the solar cycle variability for the majority of the solar VUV irradiance is about a factor of two, the underflight calibrations alone may be sufficient to track the SEE instrument degradation.

Other in-flight calibration tests include wavelength calibrations using the observed solar emission lines as reference wavelengths and field of view maps by scanning the Sun across different parts of the optics and detectors. All of the in-flight calibration tests confirm similar pre-flight calibration measurements and insure that the SEE data processing will utilize the most accurate instrumental parameters.

4. PRE-FLIGHT CALIBRATION RESULTS

The XPS pre-flight calibrations are primarily discussed in this section as the majority of the EGS pre-flight calibrations at the NIST SURF-III have not yet been performed. The XPS pre-flight calibration activities involve selecting flight detectors (photodiodes), calibrating the sensitivity of these photodiodes, performing linearity calibrations of the photodiode electronics as a function of temperature, and calibrating the visible FOV of the detectors. The Solar Aspect Sensor (SAS) calibrations include measuring the FOV of each SAS and measuring the linear variations of each SAS response as a function of incident angle.

4.1. XPS Photodiode Selection

The process of selecting the flight photodiodes for the XPS is to evaluate the photodiode for visible light leaks, to mask the outside perimeter of the photodiode, and to measure its shunt resistance. Silicon photodiodes coated with thin film filters were purchased from International Radiation Detectors (IRD), and their surfaces are first mapped to measure their visible light sensitivity. Visible light leaks, usually caused by pinholes in the coatings, are not desirable for XUV photodiodes because the solar visible radiation is about eight orders of magnitude brighter than the solar XUV radiation. The visible light maps are obtained using a red HeNe laser and by scanning the photodiode active area (10 mm x 10 mm) over the laser beam on a 0.5 mm x 0.5 mm grid. As part of the mapping procedure, the shunt resistance of the photodiode is measured. Based on these initial map results, photodiodes with low peak currents and low currents averaged over the central 7 mm x 7 mm of the photodiode are selected as candidate flight detectors.

Table 1. XPS Photodiode Visible Light Map Results and Shunt Resistances.

XP #	Filter Coating	Map Peak Current (nA)	Map Central Current (nA)	Shunt Resistance (MOhms)
1	Ti/C	0.106	0.343	17.2
2	Ti/C	0.152	< 0.1	19.6
3	Al/Sc/C	25.9	221	1000
5	Ti/Pd	3.66	155	18.2
6	Ti/Zr/Au	1.18	14.8	25.6
7	Al/Nb/C	1.80	< 1	15.9
9	Al/Mn	0.879	24.0	19.2
10	Cr/Al	2.79	60.1	23.8

The flight candidate photodiodes then have a mask, an aluminum aperture, mounted to the photodiode ceramic housing and the photodiode top surface with silver epoxy to cover the uncoated perimeter of the photodiode. This mask is required because the uncoated perimeter is too sensitive to visible light for making solar XUV measurements. After the masking process is complete, the masked photodiodes are mapped again. These second map results, along with final shunt resistance results, are the basis for selecting the best photodiodes for flight. Typically, the photodiodes with the fewest flaws in the coating and with the highest shunt resistance are selected. Table 1 shows the final visible map results and shunt resistances for the flight XUV photodiodes. The XUV Photometers (XP) numbers 4, 8, 11, and 12 are bare silicon photodiodes (IRD's AXUV-100G part number); these bare photodiodes are not listed in Table 1 because they are not mapped nor masked. The map currents are only relative values as the HeNe laser is neither regulated nor calibrated on an absolute scale. In general, the flight photodiodes do not have any pinholes in the central 7 mm x 7 mm central region and have a shunt resistance of 10 MOhms or higher.

4.2. XPS Photodiode Sensitivity Calibrations

The XPS photodiode sensitivity calibrations at PTB are obtained using the plane grating monochromator beamline²⁰ at the electron storage ring called BESSY. These PTB calibrations are based on a secondary detector standard, being a reference photodiode. The PTB reference photodiode is calibrated to the PTB primary detector standard called SYRES²¹, being a cryogenic electrical substitution radiometer. These sensitivity calibrations are performed from 0.8 to 25 nm with a typical uncertainty of 1-3%. Extra photodiodes calibrated at BESSY will also be calibrated at SURF to provide a cross-calibration between BESSY and SURF and to compare with other SURF calibrations of the prototype XPS photodiodes that will be used for the SEE underflight calibrations. The PTB results are analyzed to determine the coating thickness so that the sensitivity outside the measured spectral range can be modeled accurately for the solar irradiance calculations²². The sensitivity model uses the Henke absorption coefficients^{23,24} for the coatings and a sensitivity model of the silicon response that assumes 1 electron-hole pair per 3.63 eV of photon energy multiplied by the calculated transmission of the 5 μm silicon detecting layer. The thickness of the thin films, as shown in Table 2, are derived by fitting to the PTB measured sensitivity using a least-squares fitting algorithm. The uncertainty for the sensitivity model is estimated by the root-mean-squared (rms) difference between the measurement and the model values. An example model fit to the photodiode coated with Ti/Zr/Au is shown in Figure 3. The differences between the target and calibrated coating thicknesses in Table 2 may not be entirely physical as the modeled thickness depends strongly on the assumed density of the material, and the coating density can vary depending on the coating process. The sensitivity model also includes a 7 nm layer of silicon dioxide (SiO_2) that is deposited on the silicon top surface as a passivation layer during the manufacturing process.

Table 2. XPS Photodiode Coating Thickness.

XP #	Filter Coating	Target Thickness (nm)	Calibrated Thickness (nm)	Model Uncertainty (%)
1	Ti/C	500/50	496/45	6.16
2	Ti/C	500/50	482/48	6.19
3	Al/Sc/C	200/100/50	142/23/50	2.05
5	Ti/Pd	200/100	229/79	7.19
6	Ti/Zr/Au	20/200/100	59/204/100	3.07
7	Al/C/Nb	250/50/50	374/56/50	3.69
9	Al/Mn	200/100	187/60	0.31
10	Cr/Al	100/200	60/195	1.32

4.3. XPS Linearity Calibrations

The response of each XP electronics to input current is tested for linear variations throughout the XPS operational temperature range of -10 °C to +50 °C. A precision current source, a Keithley 236 Source Measure Unit, is connected to the XP charge amplifier in place of its photodiode. The input current is varied while the output frequency from the XP voltage frequency converter (VFC) is measured using a pulse counter, a Keithley 776 Counter/Timer. Several measurements of the

output frequency are also taken with no current input in order to obtain an average of the background (zero) level. The output count rate varies linearly with input current within a typical uncertainty of 0.2% as shown in Figure 4. As expected by the electronics design, the XP electronics become non-linear for an output count rate near 10^6 counts per sec (cps). Linearity measurements are made at different temperatures, and a temperature variation of about 0.03% per $^{\circ}\text{C}$ is typical for the XPS electronics gain.

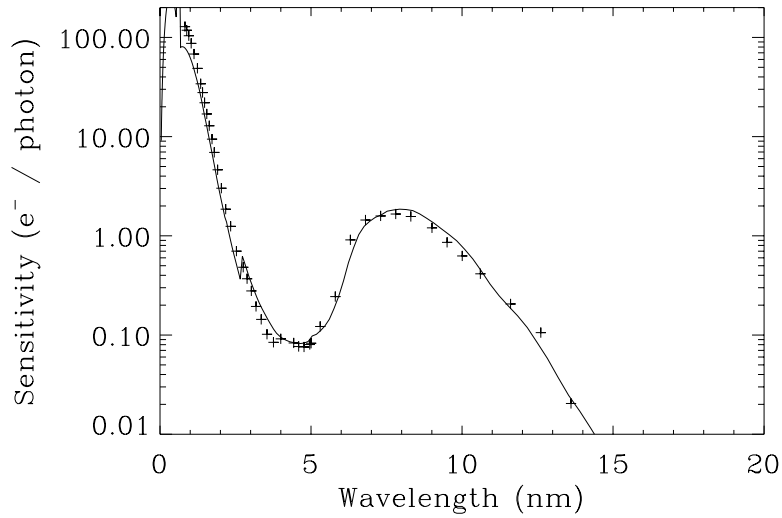


Figure 3. Comparison of Measurements and Sensitivity Model for Photodiode with Ti/Zr/Au Coating. The measurements are the plus symbols, and the model is the line.

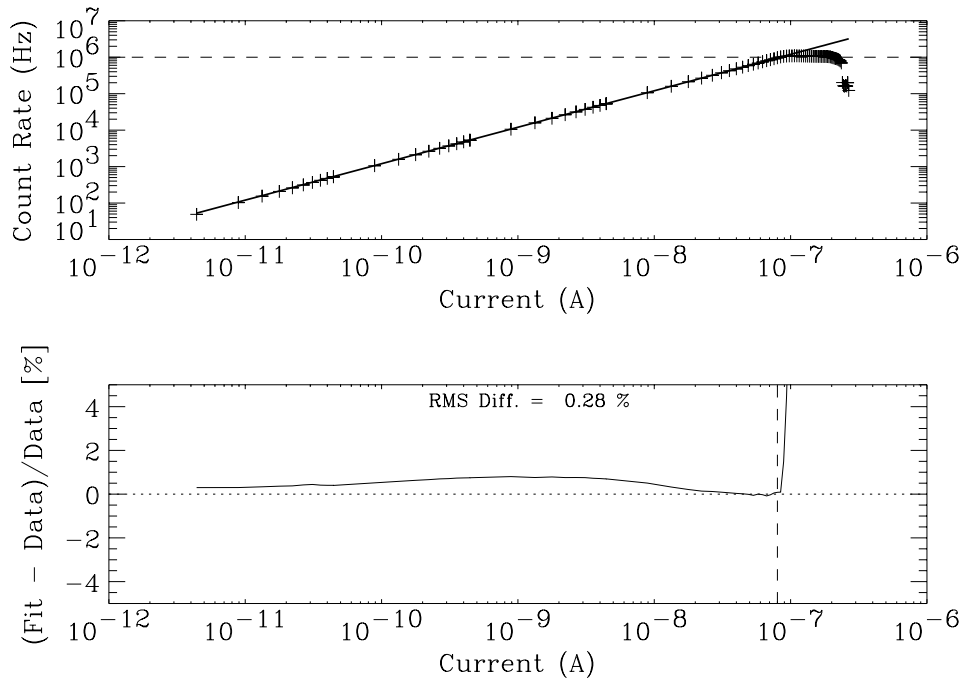


Figure 4. XP # 3 Electronics Linearity Calibration. The plus symbols are the measurements. The line in the top plot is the linear fit. The dashed line in both plots is the design limit for operation of the XP electronics (1 MHz).

4.4. XPS Visible Field of View Maps

Once the photodiodes are assembled in flight configuration inside the XPS component, visible field of view (FOV) tests are conducted to characterize the variation of the visible sensitivity as a function of incident angle. Limited FOV tests in the XUV were also obtained during the photodiode calibrations at PTB BESSY, but the primary FOV maps in the XUV will be determined using in-flight FOV scans. For the visible FOV maps, the XPS is mounted on a 2-axis gimbal table, and a 1000 Watt FEL (quartz halogen) lamp is centered on the detector under test. The lamp is placed at an appropriate distance away from the XPS to simulate a signal comparable to the solar intensity. The field of view of each detector and the transmission of the fused silica windows in the XPS filter wheel are determined over $\pm 6^\circ$ in the horizontal and vertical directions on a 1° grid. The transmission of the windows is determined as the ratio of the detector signal with a window in front of the detector to the signal without the window. Ideally, the profile of a map should be flat over its FOV, designed to be 11.3° diameter. However, the profiles of the visible FOV maps do show variations that are related to microscopic imperfections in the coating and to the geometry of the mask and aperture.

During the visible FOV tests, a reentrant light problem was discovered for the XPS. When the lamp is illuminating the photodiode near normal incidence and through a window, the light from the lamp can be reflected back onto the internal side of the window which in turn can reflect light back to the photodiode. As seen in the left plot of Figure 5, this internal reflection contributes about 1% increase to the window FOV sensitivity near normal incidence. To counteract this internal reflection, the fused silica windows are now tilted 10° relative to the photodiodes surface. This 10° tilt does eliminate the reentrant light over at least half of the XPS FOV, as can be seen in the right plot of Figure 5. There are two windows used for each photodiode, and each window's 10° tilt lies in the horizontal or vertical axis. In the right plot of Figure 5, the window 2 has its tilt in the vertical axis, and thus it has no reentrant light problem over its full FOV in the horizontal scan. A larger tilt of the window would completely eliminate the reentrant light for the window calibrations in both axes, but the 10° tilt was the largest angle allowed by the existing XPS design. With most of the FOV free of this reentrant light problem, the full FOV can be precisely calibrated using the results from the two different windows.

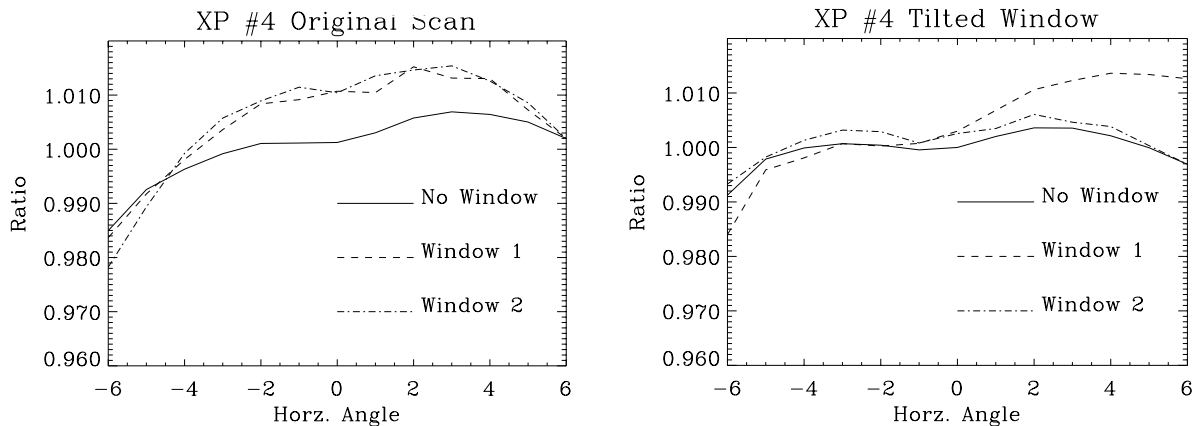


Figure 5. XP #4 FOV Horizontal Scans. The left plot shows the original configuration when the windows were parallel to the photodiode surface. The ratio is the photodiode signal normalized to the signal at the center. The ratios for the windows are also scaled up to match the no window ratio at 6° . The right plot shows the final configuration when the windows are tilted 10° with respect to the photodiode surface.

4.5. Solar Aspect Sensor Calibrations

The knowledge of the solar pointing for the SEE instruments is obtained from the Solar Aspect Sensor (SAS). The SAS is a quadrant photodiode with a square entrance aperture and with a neutral density 4.0 filter. The SAS full field of view is 15° . There are two redundant SASs, one on SSPP and one on EGS. The EGS SAS is also used to determine the FOV angles during the SURF calibrations.

Each SAS is calibrated over its FOV and over its operational temperature range of 5°C to 35°C . The derivation of the SAS conversion of angle to voltage is the primary purpose for these SAS calibrations. For the initial tests in a thermal oven, the

light source, an Oriel 77500 Fiber Optic Illuminator, is fixed, and the SAS is rotated on a rotational stage about the SAS aperture. This FOV calibration in one axis is done with offsets of -2.5° , 0° , and $+2.5^\circ$ in the other axis and then repeated for the other axis by flipping the SAS 90° on the rotational stage. These calibrations indicate that the SAS did not have any detectable temperature dependence. An additional SAS calibration was performed on a laboratory bench with a 1000 W FEL (quartz halogen) lamp in order to simulate better the brightness of the Sun. For this setup, the lamp is moved on an optical rail while the SAS is fixed for the Y axis calibration, and the lamp is fixed while the SAS is rotated by the SSPP (1-axis gimbal table) for the X axis calibration. The SAS calibrations show that the SAS outputs vary linearly with incident angle to within 0.6 arc-minutes. While some scans show linearity to within 0.3 arc-minutes as shown in Figure 6, the systematic variations near normal incidence, as caused by internal reflections between the filter and quadrant photodiode, increase the calibration uncertainty to 0.6 arc-minutes. Table 3 lists the SAS conversion factors between output volts and incident angle.

Table 3. SAS Calibration Results.

Axis	SSPP SAS	EGS SAS
X Axis (SSPP rotation axis)	1.09022 Volt/deg	1.09681 Volt/deg
Y Axis (solar track axis)	1.08661 Volt/deg	1.09176 Volt/deg

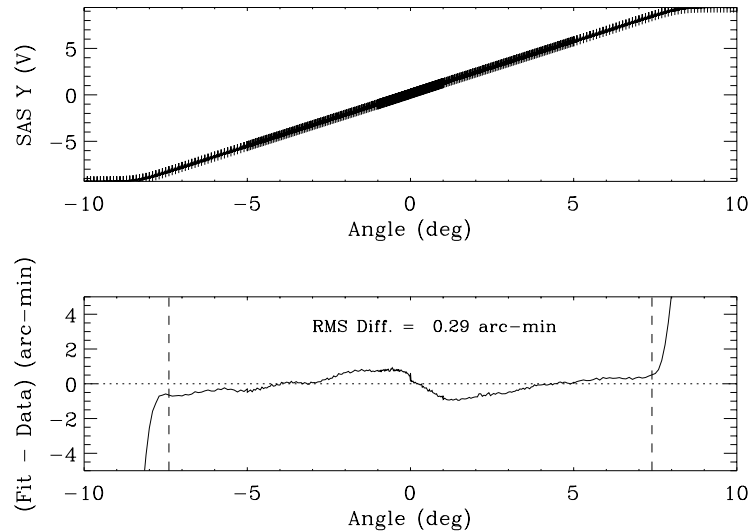


Figure 6. Example Field of View Calibration for SSPP Solar Aspect Sensor (SAS). The top plot shows the SAS output as a function of source incident angle along the SAS Y axis. The bottom plot shows the difference between the linear fit and the measured output. The output rolls over at its limiting FOV angle of 7.5° (dashed line). The variation near the center is systematic and is caused by internal reflection between the neutral density filter and quadrant photodiode.

5. SUMMARY

The pre-flight calibrations of the XPS are fully analyzed and are being incorporated into the TIMED SEE science data processing software. The analysis of the pre-flight calibrations of the EGS are still on-going as the primary NIST SURF calibrations for EGS are planned for August 1999,. An additional pre-flight calibration of the EGS at SURF is planned at the end of spacecraft Integration and Test (I&T) in March 2000. The results of the EGS pre-flight calibrations will be given in a future report.

It is critical to have well-calibrated and long-term solar VUV spectral irradiance measurements for current and future research of the solar connection to the Earth's upper atmosphere. While our recent rocket measurements provide more accurate solar irradiance reference spectra, new, more accurate satellite measurements made on a daily basis are needed to establish a long-term database of solar VUV irradiance and its variability. While the UARS solar instruments are now creating such a database for the solar VUV irradiance above 120 nm, the daily spectral measurements by the TIMED SEE may be the first satellite measurements since 1981 that are suitable for this long-term database for wavelengths below 120 nm.

ACKNOWLEDGMENTS

We thank the SEE instrument team at LASP, the TIMED spacecraft team at the Johns Hopkins University Applied Physics Laboratory (JHU APL), and the project scientists and managers at NASA for their support in developing the SEE instrument. We are grateful to Frank Scholze at PTB BESSY, Randy Canfield at NIST SURF, and Raj Korde at IRD for their assistance and useful discussions about the photodiodes for the XPS. This work is supported by JHU APL contract number JH774017.

REFERENCES

1. J. Lean, "Solar ultraviolet irradiance variations: a review", *J. Geophys. Res.*, **92**, 839, 1987.
2. J. Lean, "Variations in the Sun's radiative output", *Reviews of Geophysics*, **29**, 505, 1991.
3. G. J. Rottman, "Results from Space Measurements of Solar UV and EUV Flux", *Solar Radiative Output Variation*, P. Foukal (Ed.), 71, Cambridge Research and Instrumentation Inc, Boulder, 1987.
4. R. G. Roble, E. C. Ridley, A. D. Richmond, and R. E. Dickinson, "A coupled thermosphere / ionosphere general circulation model", *Geophys. Res. Lett.*, **15**, 1525, 1988.
5. A. E. Hedin, "Extension of the MSIS thermosphere model into the middle and lower atmosphere", *J. Geophys. Res.*, **96**, 1159, 1991.
6. T. N. Woods, F. G. Eparvier, S. M. Bailey, S. C. Solomon, G. J. Rottman, G. M. Lawrence, R. G. Roble, O. R. White, J. Lean, and W. K. Tobiska, "TIMED Solar EUV Experiment", *SPIE Proceedings*, **3442**, 180, 1998.
7. L. R. Canfield and N. Swanson, "Far ultraviolet detector standards", *J. of Res. of the National Bureau of Standards*, **92**, 97, 1987.
8. J. H. Walker, R. D. Saunders, J. K. Jackson, and D. A. McSparron, "The NBS scale of spectral irradiance", *J. of Res. of the National Bureau of Standards*, **93**, 7, 1988.
9. A. C. Parr and S. Ebner, *SURF II User Handbook*, NBS Special Publication, Gaithersburg, 1987.
10. T. N. Woods, G. J. Ucker, and G. J. Rottman, "SOLAR STellar Irradiance Comparison Experiment I : 2. instrument calibration", *J. Geophys. Res.*, **98**, 10,679, 1993.
11. T. N. Woods, R. T. Wrigley, G. J. Rottman and R. E. Haring, "Scattered light properties of diffraction gratings", *Applied Optics*, **33**, 4273, 1994.
12. T. N. Woods and G. J. Rottman, "Solar EUV Irradiance Derived from a Sounding Rocket Experiment on 10 November 1988", *J. Geophys. Res.*, **95**, 6227, 1990.
13. T. N. Woods, G. J. Rottman, S. Bailey, and S. C. Solomon, "Vacuum-ultraviolet instrumentation for solar irradiance and thermospheric airglow", *Optical Eng.*, **33**, 438, 1994.
14. R. Korde and J. Geist, "Quantum efficiency stability of silicon photodiodes", *Applied Optics*, **26**, 5284, 1987.
15. R. Korde, L. R. Canfield, and B. Wallis, "Stable high quantum efficiency silicon photodiodes for vacuum ultraviolet applications", *SPIE Proceeding*, **932**, 153, 1988.
16. L. R. Canfield, J. Kerner and R. Korde, "Stability and quantum efficiency performance of silicon photodiode detectors in the far ultraviolet", *Applied Optics*, **28**, 3940, 1989.
17. R. Korde and L. R. Canfield, "Silicon photodiodes with stable, near theoretical quantum efficiency in the soft x-ray region", *SPIE Proceeding*, **1140**, 126, 1989.
18. L. R. Canfield, R. Vest, T. N. Woods, and R. Korde, "Silicon photodiodes with integrated thin film filters for selective bandpasses in the extreme ultraviolet", *SPIE Proceedings*, **2282**, 31, 1994.
19. S. M. Bailey, T. N. Woods, C. A. Barth, and S. C. Solomon, "Measurements of the solar soft x-ray irradiance from the Student Nitric Oxide Explorer", *Geophys. Res. Letters*, **26**, 1255, 1999.
20. F. Scholze, M. Krumrey, and D. Fuchs, "Plane grating monochromator beamline for VUV radiometry", *Rev. Sci. Instrum.*, **65**, 3229, 1994.
21. H. Rabus, V. Persch, and G. Ulm, "Synchrotron-radiation-operated cryogenic electrical-substitution radiometer as the high-accuracy primary detector standard in the ultraviolet, vacuum ultraviolet, and soft x-ray spectral ranges", *Appl. Optics*, **36**, 5421, 1997.
22. S. M. Bailey, T. N. Woods, L. R. Canfield, R. Korde, C. A. Barth, S. C. Solomon, and G. J. Rottman, "Sounding rocket measurements of the solar soft x-ray irradiance", *Solar Physics*, in press, 1999.
23. B. L. Henke, P. Lee, T. J. Tanaka, R. L. Shimabukuro, and B. K. Fujikawa, "Low-energy x-ray coefficients: photoabsorption, scattering, and reflection", *At. Data Nucl. Data Tables*, **27**, 1, 1982.
24. B. L. Henke, J. C. Davis, E. M. Gullikson, and R. C. C. Perera, *A Preliminary Report on X-ray Photoabsorption Coefficients and Atomic Scattering Factors for 92 Elements in the 10-10,000 eV Region*, Lawrence Berkeley Laboratory Report LBL-26259, Berkeley, 1988.

